**IRAQI BULLETIN OF GEOLOGY AND MINING (IBGM)\
IRAQ GEOLOGICAL SURVEY (GEOSURV-IRAQ)**

Vol.20, No.1, 2024 ***p 43 – 51***

SEISMICITY AND FOCAL MECHANISM ANALYSIS OF THE LOCAL EARTHQUAKES IN THE ZAGROS FOLD-THRUST BELT OF THE IRAQI KURDISTAN REGION

Omar Qadir Ahmed[1*], and Ahmed Muslim Attallah Khawaja[2]

[1] Department of Geology, College of Science-Sulaimani University, Iraq;
[*]Correspondence e-mail: omar.ahmed@univsul.edu.iq
[2] Department of Applied Geology, College of Science- University of Babylon, Iraq.
e-mail: sci.ahmed.moslem@uobabylon.edu.iq

Type of the Paper: Article
Received: 27/ 01/ 2023
Accepted: 07/ 03/ 2023

Keywords: Seismicity of Iraq; Moment tensor solution; Zagros mountains; Stress analysis.

ABSTRACT

During the period of 2020 to May 2022, the Iraqi Kurdistan region experienced several small to moderate size earthquakes. The seismic waveform data of these earthquakes were collected from regional and local broadband seismic stations. Waveform data was analyzed for seventy earthquakes to determine their source parameters, which may contribute to the active tectonics in those areas. Moment tensor inversion is estimated for the detected local earthquakes by analysis of observed seismic waveforms in different selected areas. The waveform inversion determines the seismic moment, depth, and kind of rupturing fault at the source. A grid search is employed as part of the inversion procedure across the strike, dip, and rake angles for each depth between 0.5 and 40 Km in increments of 1 Km. Waveform modeling is used to correlate the observed and created waveforms by applying bandpass filters and a suitable velocity model for Green's function using computer programs in seismology and the ISOLA code "Isolated asperities" for multiple-point source modeling. The results show that the earthquakes with $M \geq 4$ have a focal depth ranging between 7 and 20 Km. Furthermore, the regional stresses were identified and the mechanism for the optimum fit was determined. The source mechanisms in the study area are most likely a combination of strike-slip, oblique-slip, and thrust.

1. INTRODUCTION

The study area, the Iraqi Kurdistan region, is situated where the Arabian and Eurasian tectonic plates collide and the intense seismicity related to the ongoing convergence (Abdulnaby, 2019). According to the tectonic divides of Iraq, Sulaymaniyah is situated in northeastern Iraq inside the Zagros Fold-Thrust Belt (ZFTB), which causes frequent earthquakes in northern and eastern Iraq (Figure 1). The Thrust Zone was described by Numan (2001) as a set of normal faults in the basement rocks beneath the sedimentary cover and subduction tectonic facies of the Zagros Thrust and the mechanics of the collision between the Arabian and Eurasian plates control the active faults in the study area.

For a Fold and Thrust Belt, the seismicity rates in the Zagros collision zone are among the highest in the globe (Tatar et al., 2004). The majority of the moderate-to-large historical earthquakes in eastern Iraq have occurred along this belt (Alsinawi & Banno, 1976). Moderate

magnitude earthquakes occur in the study area with the focal depth ranging from 6 to 25 Km. In the study area, few studies of source analysis have been conducted. These studies reported a strike-slip mechanism with a reverse component (Khalid J. Fahmi, Mazin A.H. Al Salim and Basil S. Ayar, 1986), and NE and NW trending reverse faulting (Kim & Nuttli, 1977).

According to Gök et al. (2008), the northern Arabian Platform's crust is stable. As a result, the differences in crustal thickness in the ZFTB demonstrate the tectonic evolution of the area, where the Arabian and Eurasian tectonic plates collide. Mohammed & Al-Rahim (2020) noted that the spatial differences between the tectonic regime and the stress field are compatible with the neotectonic stress field. The crustal structure (Moho depth) beneath the ANB1 station is 44 Km (Rafea et al., 2022).

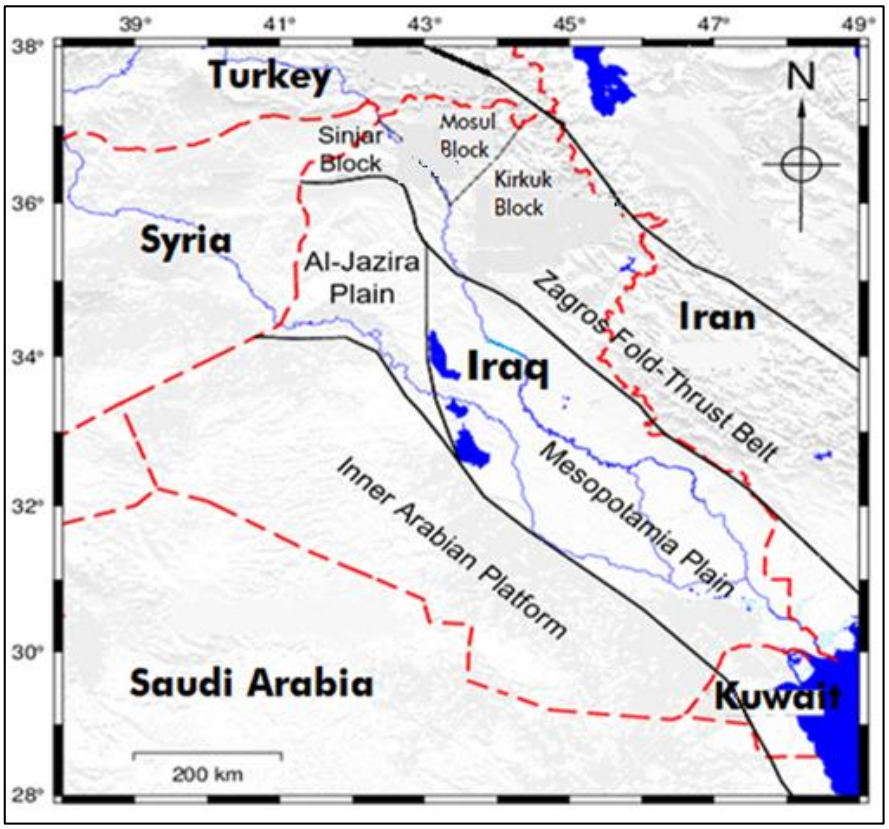

Figure 1: The tectonic divisions of Iraq and the three basement blocks of the Zagros fold-thrust belt (K Al-Azzawi, 2013).

2. DATASETS

Many earthquakes have been recorded by the SLY1 broadband station, at a rate of 100 samples per second. Seismic waveforms of seventy small-moderate earthquakes were analyzed that occurred during the period from November 2020 to May 2022 with magnitudes ≥ 1.6 Mw. Datasets of these earthquakes were collected from the Kandilli Observatory (KO), Incorporated Research Institutions for Seismology (IRIS), the International Seismological Centre (ISC), the Iranian Seismological Center (IRSC) as well as from (SLY1, KIR1, DHK1, ANB1, and KAR2) broadband seismic stations of the Mesopotamian Seismic Network (MPSN) that is operated by the Seismological Laboratory of the University of Basrah (SLUB). Figure 2 shows the location of the local and regional broadband seismic stations used in this study. These data were collected to ascertain the focal mechanism analysis (FMA).

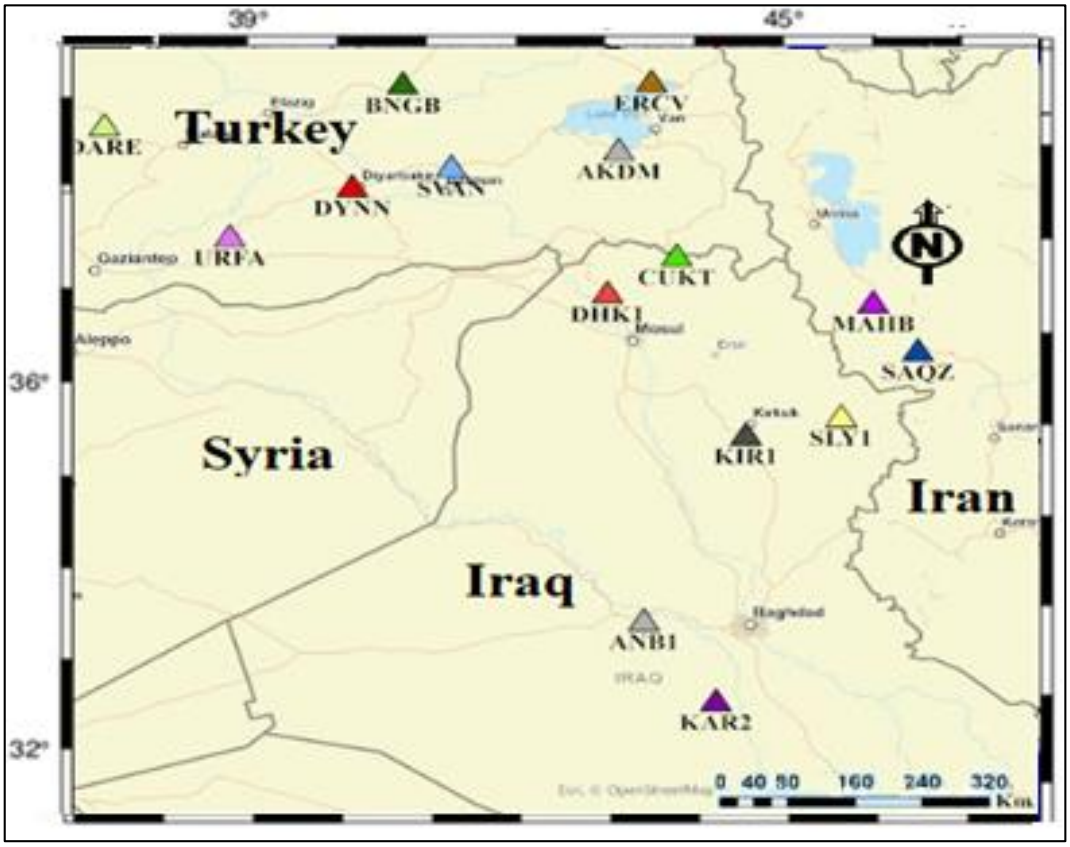

Figure 2: The location of the local and regional broadband seismic stations used in this study.

Table 1 shows the earthquakes with magnitude magnitude ≥ 4 that occurred in the study area.

Table 1: Analyzed earthquakes that occurred for the period from Nov 2020 to May 2022 in the with Mw ≥ 4.

No	Date	Origin time (UTC)	Lat. Deg.	Long. Deg.	Depth (km)	Magnitude (Mw)
1	2020/11/09	23:18:25	35.46	45.10	10	4.9
2	2021/02/11	22:10:34	34.62	45.29	9	4.8
3	2021/04/06	15:12:25	35.66	45.99	9.3	5.2
4	2021/07/31	23:41:21	34.52	45.28	8	4.3
5	2021/09/08	15:43:05	34.77	45.22	22	4.4
6	2021/09/24	23:43:12	34.61	45.62	10	4.3
7	2022/01/10	18:29:48	35.63	44.86	15	4.5
8	2022/01/10	20:11:16	35.7	45.00	10	4.6
9	2022/04/16	19:00:24	34.53	45.43	14	4.0
10	2022/05/29	5:52:45	34.64	45.62	10	4.1
11	2022/05/30	1:23:38	34.59	45.57	6.1	4.2

For (FMA)s to be accurately identified, the locations, depths, and magnitudes are essential. It is necessary to convert the original seismic data format into the SAC and GSAC forms. Before running the analysis software, the header file for each data file has to be prepared. These selected earthquakes are displayed in Figure 3.

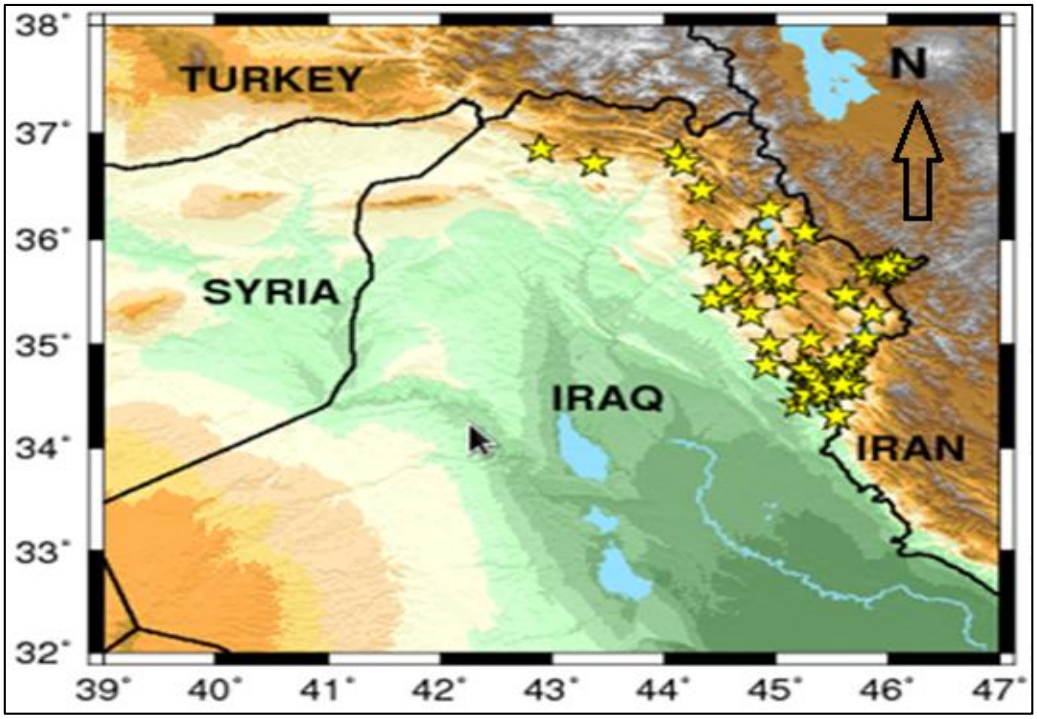

Figure 3: The earthquakes' epicenter in the study area from Nov 2020 to May 2022.

The recording in the local stations is done for the simultaneous movement as a function of advancing time in three directions: Z, N, and E. SLY1 and DHK1 are close to the Zagros Mountains.

The latitude and longitude of the local and regional used stations are shown in Table 2. The work aims to advance our understanding of the seismic activity in the studied area using seismic data from 16 broadband seismic stations.

Table 2: The broadband seismic stations that were used.

Station code	Network	Latitude (º)	Longitude (º)	Elevation (m)
SLY1	ISO	35.57	45.36	756
KIR1	ISO	35.38	44.34	331
DHK1	ISO	36.86	42.86	766
ANB1	ISO	33.40	43.25	53
KAR2	ISO	32.53	44.02	43
AKDM	KO	38.32	42.98	1662
CUKT	KO	37.24	43.60	1298
BNGB	KO	38.99	40.67	1180
DARE	KO	38.57	37.48	1080
YBB	KO	37.95	40.13	657
ERCV	KO	39.01	43.33	1679
ERZN	KOI	39.58	39.72	1317
SAQZ	IRSC	36.26	46.18	2146
SVAN	KO	38.15	41.19	650
MAHB	IRSC	36.76	45.7	1370
URFA	KO	37.44	38.82	938

3. METHODOLOGY

The regional seismic moment tensor inversion (MTI) method was used in this study to estimate FMA and moment magnitudes for (11) earthquakes (Figure 4) with magnitudes larger than 4, which was carried out using full waveform data or amplitude ratios (Havskov & Ottemoller, 2010). A theoretical seismogram must be created using complete seismograms (Shearer, 2009). A package of Computer Program in Seismology (CPS) by Herrmann et al., (2005) and an ISOLA software package (Zahradník & Sokos, 2018) were used. The most advanced methods of FMA include complete seismograms, which use earthquakes with magnitudes of three or higher. Available data and the azimuthal deployments of stations around the earthquake source determine the quality of the moment tensor inversion (Kayal, 2008).

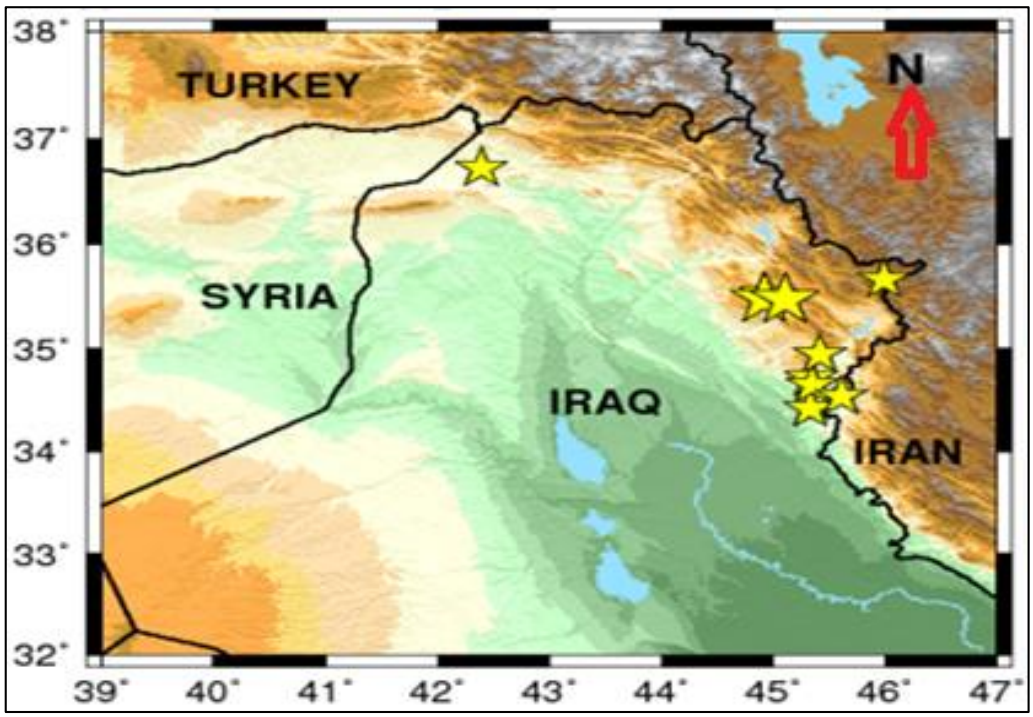

Figure 4: The quakes (yellow stars) with M > = 4.0 for the period from Nov 2020 to May 2022.

To determine the fault orientation for various event sources in the area and to provide a better evaluation of the seismic moment energy released by earthquakes, the waveform inversion (grid search) technique was applied. The moment magnitude (Mw), Seismic Moment (Mo), and data for the seismic source process are obtained by this procedure (Dahm, 1996). Using the CPS program, Green's function for the study area was calculated using the flat velocity model, which was adapted from Mooney et al. (1998) and Abdulnaby et al. (2012). To match the waveforms and determine the earthquake's moment magnitude, a suitable regional velocity model must be used (Herrmann, 2011).

The following event started 2022/01/10 at 18:29:48 UTC is presented to demonstrate the data processing and estimating of the moment tensor inversion using broadband seismic waveforms. The focus of the quake lay in the Earth's interior below Chamchamal area at latitude 35.63 and longitude 44.86. The waveform display of the event, the location of the event, and the stations used for the waveform inversion (SLY1, KIR1, DHK1, CUKT, AKDM, and BNGB) are shown in the next Figure 5.

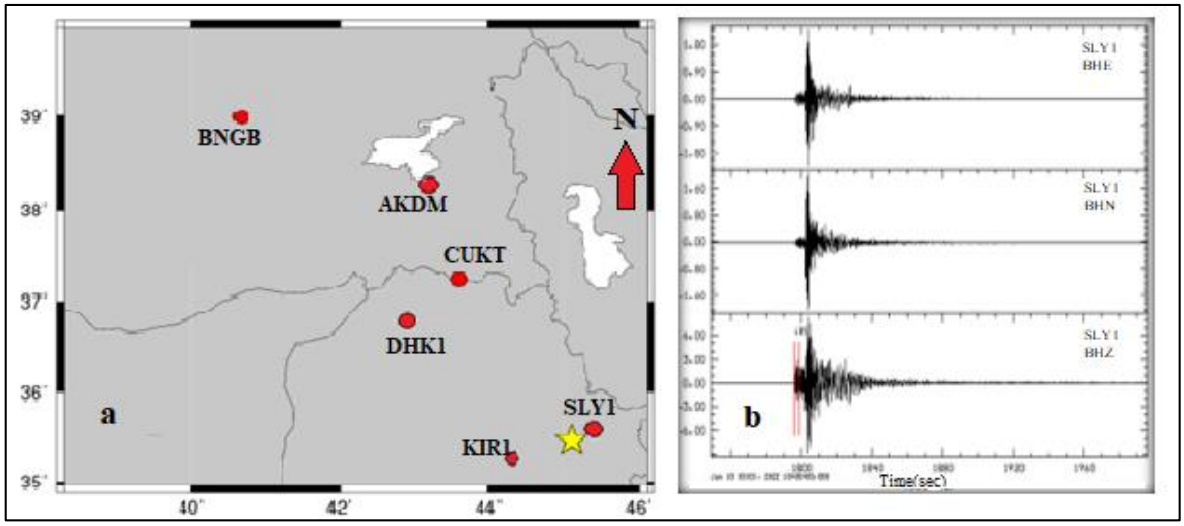

Figure 5: **a**) The earthquake location (yellow star) at latitude 35.63 and longitude 44.86 of 2022/01/10 at 18:29:48 UTC recorded in the (BB) seismic stations (red circles), and (**b**) the three components of the waveform; BHZ, BHN, and BHE in SLY1 observatory.

The software wvfgrd96 was used to determine the focal mechanism, depth, and seismic moment (Herrmann, 2015). The focal depths and fault plane solutions were estimated, the dominant mechanism of the fault displacements was derived, and the moment tensor was estimated using pre-computed Green's function for the selected earthquakes with a magnitude greater than 4. Figure 6 depicts the comparison of observed (red) and predicted (blue) waveforms for the earthquake of 2022/01/10 at 18:29:48UTC.

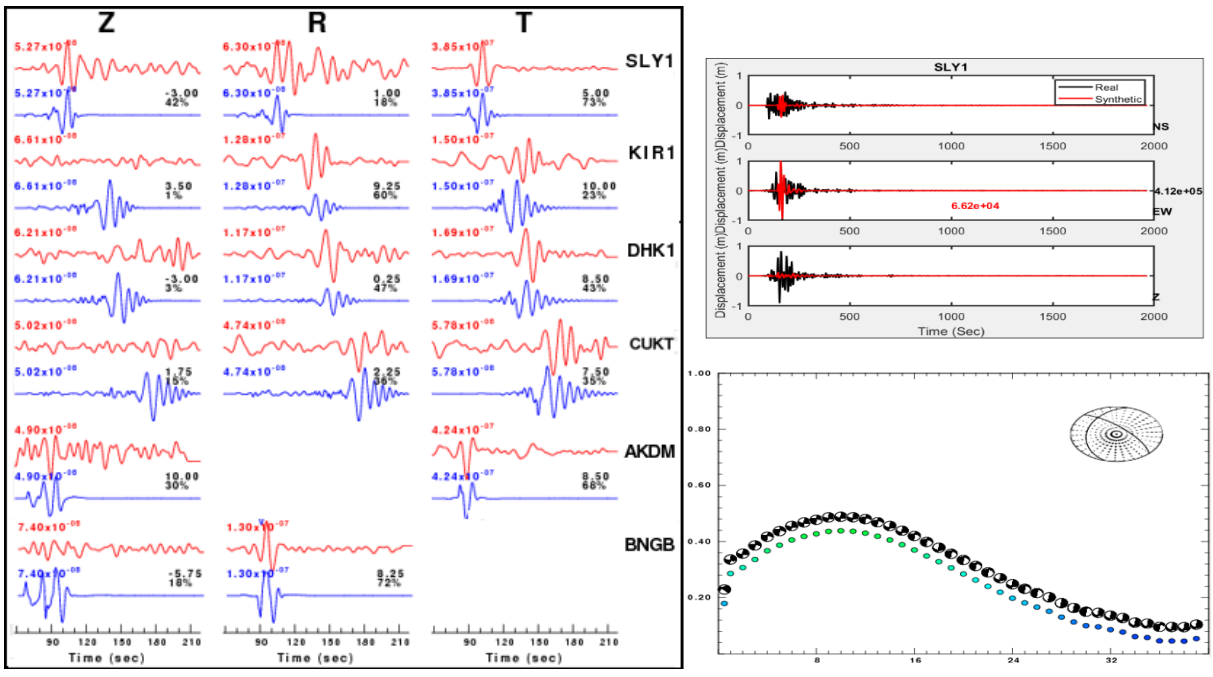

Figure 6: (**a** and **b**) Observed (red) and predicted (blue) waveforms for the earthquake of 2022/01/10 18:29:48UTC as a function of absolute travel time.
(**c**) the fit as a function of depth.

On each trace, the peak amplitude is displayed and includes the station name to the right and the peak amplitude to the left. The beach ball displays the optimal mechanisms for each source depth and the best solution at this depth. The utmost limit of the focal depth search is 39 Km, and the ideal fit is a value of 1.0.

The time shift of the synthetic in relation to the observed is given to the right of each trace at the top and the percent of fit at the bottom.

The depth sensitivity for the waveform mechanism is calculated and the optimal fit is for a depth of 16 Km. Noise from site effects and instruments may have caused some traces to be erased, i.e., in AKDM or BNGB stations, only the vertical Z component remained, while traces R or T components were rejected.

4. RESULTS AND CONCLUSIONS

The results of this study show that the broadband stations are used efficiently for determining source parameters of earthquakes of magnitude equal and/or greater than 4 in regions with moderate seismicity. In general, the waveform inversion results for most of the earthquakes indicate that the responsible fault was mostly a strike-slip fault, although some dip-slip faults were estimated. In comparison between the computed focal mechanisms for the same event for example the event that occurred in (Jan-10-2022) and recorded by local stations; (SLY1), (KIR1), and (DHK1), respectively, the fit is not equally well. The focal mechanism solution resulting from SLY1 records using the ISOLA and CPS programs throughout the stages of processing gave more waveform matching percentages because this event occurred nearer to SLY1 than to KIR1 and DHK1. The time differences between the observed and predicted traces are possible, which arise in the processing of waveform matching for the assumed source location.

Furthermore, the results reveal that the earthquakes with M > 4 have a focal depth ranging between 7 to 20 Km. The calculated seismic moment values range from (1.17) to (4.22). The measured dips range between 10° and 90°, and the rakes between (-175° – 170°). The estimated focal depth for the event that occurred on January 10, 2022, at (18:29:48) is 14 Km, while the estimated focal depth for the event that occurred on September 8, 2021, is 20 km. Rake is the direction the hanging wall moves during rupture, measured relative to the fault strike (between -180 and 180 decimal degrees). A rake of 0° means the hanging wall or the right side of a vertical fault moved away from the observer in the strike direction. Furthermore, the dip (90°) with a rake equal (0) means left lateral strike-slip. The source mechanisms in the study area are most likely a combination of strike-slip, oblique-slip, and thrust. The main compressional directions are NNE – SSW, NW – SE, and NE – SW. They have shallow focal depths of less than 20 Km at crustal depths due to regional compressive stresses through the moment tensor calculation process. Most of the earthquakes are concentrated in the ZFTB and some of the events occurred near Khanaqin and Mandeli-Badra area. The software selected the best-fit solution, plotted the best moment tensor solution, and computed values (e.g., magnitude, depth, strike, dip, and rake) relevant to the earthquake. The moment tensor solutions have a quality factor assigned by the number of stations used during the inversion and the goodness of fit between synthetic and observed data. It can be inferred from the results that these earthquakes occurred in the lower part of the upper crust.

The results of source mechanisms and stress orientations for the selected earthquakes with magnitudes greater than 4 are displayed in Figure 7. For each depth between 0.5 and 39 Km in steps of one km, a grid search across the strike, dip, and rake angles was utilized. Different source mechanisms are characterized by different radiation patterns of seismic wave energy.

The outcomes of the moment tensor inversion, source parameters, earthquake rupture orientation, and propagation direction of the analyzed events with M ≥ 4 are shown in Table 3.

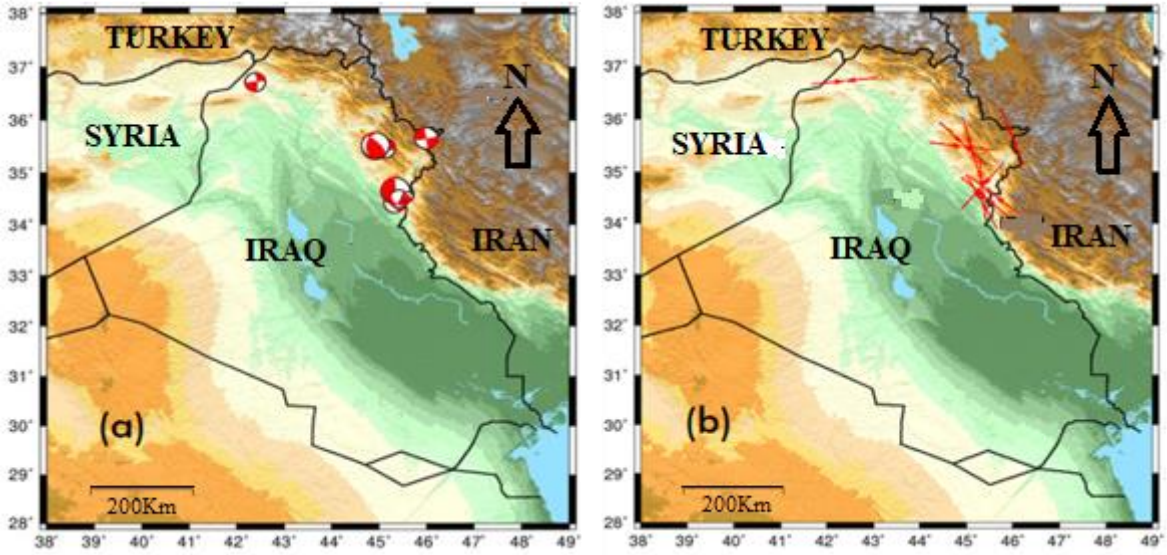

Figure 7: (**a**) The focal mechanism solutions for ten earthquakes in the study area, and (**b**) Stress orientations.

Table 3: Source parameters for the earthquakes with M > 4 in the study area.

Event date	Origin Time	Strike	Dip	Rake	Strike$_2$	Dip$_2$	Rake$_2$	m_0	Mw	Z (Km)
2020/11/09	23:18:25	98	80	-165	5	75	-10	1.17E+22	4.9	9
2021/02/11	22:10:34	47	45	95	220	45	85	4.02E+21	4.8	10
2021/04/06	15:12:25	170	90	-175	80	85	0	4.22E+22	5.2	10
2021/07/31	23:41:21	152	67	99	310	25	70	1.50E+22	4.3	8
2021/09/08	15:43:05	175	90	-100	85	10	0	1.88E+24	4.4	20
2021/09/24	23:43:12	264	85	165	355	75	5	2.76E+21	4.3	9
2022/01/10	18:29:48	315	70	60	194	36	44	4.03E+23	4.5	14
2022/01/10	20:11:16	10	80	15	277	75	170	1.93E+23	4.6	9
2022/05/29	5:52:43	30	80	-50	132	41	-165	4.10E+21	4.1	9
2022/05/30	1:23:38	310	70	70	177	28	133	1.55E+19	4.2	7

ACKNOWLEDGMENTS

Thanks to Dr. Robert Herrmann for his software package. Thanks go to IRIS and ISN for the seismic data and catalog for this research. The author is grateful to the staff of the Mesopotamian Seismic Network (MPSN) in Basrah-Iraq for their data and scientific support.

REFERENCES

Abdulnaby, W. (2019). *Structural Geology and Neotectonics of Iraq, Northwest Zagros*. 53–73. https://doi.org/10.1016/b978-0-12-815048-1.00004-4

Abdulnaby, W., Mahdi, H., & Al-Shukri, H. (2012). Crustal structure from joint inversion of receiver function and surface wave dispersion beneath Duhok, NW Iraq. *Istanbul 2012-International Geophysical Conference and Oil & Gas Exhibition*, 1–4.

Alsinawi, S. A., & Banno, I. S. (1976). The first microearthquake recording in Iraq. *Tectonophysics*, *36*(4), T1–T6.

Dahm, T. (1996). Relative moment tensor inversion based on ray theory: theory and synthetic tests. *Geophysical Journal International*, *124*(1), 245–257.

Gök, R., Mahdi, H., Al-Shukri, H., & Rodgers, A. J. (2008). Crustal structure of Iraq from receiver functions and surface wave dispersion: implications for understanding the deformation history of the Arabian–Eurasian collision. *Geophysical Journal International*, *172*(3), 1179–1187.

Havskov, J., & Ottemoller, L. (2010). *Routine data processing in earthquake seismology: with sample data, exercises and software*. Springer Science & Business Media.

Herrmann, R. B. (2011). *Computer Programs in Seismology Training Course Moment Tensor Inversion*. Seismological Society of America. https://www.eas.slu.edu/eqc/eqc_cps/WORKSHOP_MT_1/MomentTensorCourse.pdf

Herrmann, R. B. (2015). *Computer Programs in Seismology Moment Tensor Inversion VirtualBox VDI Distribution* (p. 65). https://ds.iris.edu/media/workshop/2015/09/iris-international-development-seismology/files/presentations/MomentTensor2015_01.pdf

Herrmann, R. B., Jeon, Y. S., & Yoo, H. J. (2005). Broadband source inversion using digital data from Korean seismic networks. *Proc. 4th International Seminar on Seismic Tomography of Far-East Asia and Related Words*, *2*.

K Al-Azzawi, N. (2013). Paleo and Neo-Tectonics of the Mosul Fault and its Impact on the Tectonics of the Foreland Area of Iraq. *Iraqi National Journal of Earth Science*, *13*(1), 59–74.

Kayal, J. R. (2008). *Microearthquake seismology and seismotectonics of South Asia*. Springer Science & Business Media.

Khalid J. Fahmi, Mazin A.H. Al Salim and Basil S. Ayar. (1986). Recent earthquake activity in the lesser Zab region of northeastern Iraq. *Tectonophysics*, *131*, 89–111.

Kim, S. G., & Nuttli, O. W. (1977). Spectral and magnitude characteristics of anomalous Eurasian earthquakes. *Bulletin of the Seismological Society of America*, *67*(2), 463–478.

Mohammed, H. J., & Al-Rahim, A. M. (2020). Evaluation stress field and tectonic regime In Mid-Eastern Iraq-Western Iran from the inversion of moment tensor focal mechanism data. *The Iraqi Geological Journal*, 120–135.

Mooney, W. D., Laske, G., & Masters, T. G. (1998). CRUST 5.1: A global crustal model at 5× 5. *Journal of Geophysical Research: Solid Earth*, *103*(B1), 727–747.

Numan, N. M. S. (2001). Discussion on "Dextral transpression in Late Cretaceous continental collision, Sanandaj–Sirjan Zone, western Iran": [Journal of Structural Geology, 22(8) (2000) 1125–1139]. *Journal of Structural Geology*, *23*(12), 2033–2034. https://doi.org/https://doi.org/10.1016/S0191-8141(01)00075-X

Rafea, H. F., Al-Heety, E. A. ., & Abdulnaby, W. (2022). Crustal velocity structure of Western Iraq from inversion of receiver functions at Anbar seismic station. *The Iraqi Geological Journal*, 25–34.

Shearer, P. M. (2009). *Introduction to Seismology* (2nd ed.). Cambridge University Press. https://doi.org/DOI: 10.1017/CBO9780511841552

Tatar, M., Hatzfeld, D., & Ghafory-Ashtiany, M. (2004). Tectonics of the Central Zagros (Iran) deduced from microearthquake seismicity. *Geophysical Journal International*, *156*(2), 255–266.

Zahradník, J., & Sokos, E. (2018). ISOLA code for multiple-point source modeling. *Moment Tensor Solutions: A Useful Tool for Seismotectonics*, 1–28.